A Real-Time PHIL Implementation of a Novel Nonlinear Distributed Control Strategy for a Multi-Terminal DC Microgrid

Ömer Ekin, Filipe Perez, Gilney Damm, Veit Hagenmeyer

A Real-Time PHIL Implementation of a Novel Nonlinear Distributed Control Strategy for a Multi-Terminal DC Microgrid

1st Ömer Ekin
Institute for Automation and Applied Informatics (IAI)
Karlsruhe Institute of Technology (KIT)
Karlsruhe, Germany

2nd Filipe Perez
L2S Laboratory
Paris-Saclay University
Gif-sur-Yvette, France

3rd Gilney Damm
IMSE Laboratory
University Gustave Eiffel
Marne-la-Vallée, France

4th Veit Hagenmeyer
Institute for Automation and Applied Informatics (IAI)
Karlsruhe Institute of Technology (KIT)
Karlsruhe, Germany

***Abstract*—Multi-terminal DC Microgrids have great potential for integrating Renewable Energy Sources, Storage Technologies, and modern loads more efficiently because most of them operate on DC power. Besides the reduced conversion steps between the components, which avoids considerable losses, multi-terminal DC MicroGrids offer advantages due to the lack of skin effects and reactive power. Nevertheless, stabilizing such a DC network by controlling its power converters is a very challenging task in view of the fact that the classical solution, to use PI controllers based on linearized models, may lead to stable behavior only in a small region around the respective equilibrium point. In this paper, we present a real-time PHIL implementation of a novel nonlinear control scheme for a multi-terminal DC MicroGrid. The amount of needed capacitors is reduced significantly concerning previous approaches. The proposed nonlinear controller is compared with a cascaded PI controller based on a linearized model, the so-called vector control. Both approaches, nonlinear and linear, are implemented and validated on a real PHIL multi-terminal DC MicroGrid consisting of a battery, a PV, and two load ports. The real-time experimental results of PI-based and nonlinear control-based DC Microgrids are then compared. They show that the nonlinear control allows to better deal with disturbances and nonlinearities of the system, for several points of operation without re-tuning.**

I. Introduction

The large majority of Renewable Energy Sources (RES) and energy storage devices have native use of Direct Current (DC) power, and therefore must be connected to the utility grid through power converters [1]. In the same way, a large share of loads (electric vehicles for example) converts Alternating Current (AC) back to Direct Current for use. These features have brought DC MicroGrids into the focus of research [2]–[5].

In these DC Microgrids, conversion to AC between generators, storage, and consumers is omitted. This avoids conversion losses and also Electro-Magnetic Compatibility (EMC) problems resulting from rapid switching of power semiconductors when converting DC to AC. In addition, DC Microgrids are easier to be regulated due to the lack of reactive power, frequency regulation, synchronization, and power factor [6], [7]. Additionally, in the case of multi-terminal DC networks, lines can be utilized significantly more, since neither skin effects nor reactive power occurs during the transmission of Direct Current [8]–[10]. Furthermore, such Microgrids will most likely become ubiquitous in the near future as an important link between intermittent distributed generation and loads naturally in DC, and the main distribution grid in AC [11]. Such DC Microgrids will become dispatchable clusters, with local storage and local AC grids, that will be much easier to integrate into the legacy AC transmission grid.

Unfortunately, the construction of such DC Microgrids implies the connection of large numbers of power converters, which can be a very difficult task. Indeed, such power converters act as constant power loads, behaving as negative impedances, which may lead to instability [12]. This is particularly true when using industrial standard PI controllers [13], [14]. For this reason, it is important to develop nonlinear controllers for these DC Microgrids [15], [16].

In this paper, we present a real-time PHIL-implemented nonlinear controller for a particular multi-terminal DC MicroGrid that can well represent a residential grid composed of local renewable energy sources (e.g. PVs), storage (e.g. batteries), and DC loads (e.g. electric vehicles). Model The proposed control scheme is based on previous theoretical results [17], [18], and is further developed, in the present paper, for the experimental level. The number of needed capacitors in [17], [18] is reduced significantly and a more robust design with respect to system shutdowns based on fuses or system breakers is achieved. Based on the new system architecture, a new nonlinear control algorithm is derived. The proposed multi-terminal DC MicroGrid architecture and the control algorithm are validated and verified on a real-time PHIL DC MicroGrid consisting of a battery, a PV, and two

This work was supported by the Helmholtz Association under the program "Energy System Design".

load ports at the Smart Energy System Control Laboratory [19]. A comprehensive comparison with a PI controller is undertaken using the PHIL setup.

This paper is organized as follows. Section II introduces the multi-terminal DC MicroGrid setup and its model derived for the respective control tasks. Section III presents the Control Algorithms used throughout this paper. Section IV describes the Experimental Setup used for the real-time PHIL implementation. Section VI then highlights the results from the PHIL experiments and compares the two established Control Algorithms. Finally, in Section VI our conclusions are presented and an outlook is given.

II. MicroGrid Model

The developed multi-terminal DC MicroGrid consists of a PV Module, a battery, and 2 EV loads as depicted in Fig. 1. Compared to previous approaches [17], [18], the capacitors on the component side are omitted here for the following reason: The capacitors on the component side can lead to high currents between the inductor and them. Safety Mechanisms of the real-time PHIL System are triggered to turn off the system for such high currents. The real-time PHIL implementation without capacitors on the components sides has shown a reduction in system failures due to safety mechanisms. Furthermore, the reduction of capacitors also has the advantage of reducing costs.

This system is modeled by the following average state-space equations:

$$\dot{I}_{Bat} = \frac{V_{Bat}}{L_{Bat}} - \frac{R_{Bat}+R_{01}}{L_{Bat}} I_{Bat} - \frac{V_{C_{Bat}}}{L_{Bat}} u_1 \tag{1}$$

$$\dot{V}_{C_{Bat}} = \frac{V_{dc}-V_{C_{Bat}}}{C_{Bat}R'_{Bat}} - \frac{V_{C_{Bat}}}{C_{Bat}R'_{Bat}} + \frac{I_{Bat}}{C_{Bat}} u_1 \tag{2}$$

$$\dot{I}_{PV} = \frac{V_{PV}}{L_{PV}} - \frac{R_{PV}+R_{02}}{L_{PV}} I_{PV} - \frac{V_{C_{PV}}}{L_{PV}} u_2 \tag{3}$$

$$\dot{V}_{C_{PV}} = \frac{V_{dc}}{C_{PV}R'_{PV}} - \frac{V_{C_{PV}}}{C_{PV}R'_{PV}} + \frac{I_{PV}}{C_{PV}} u_2 \tag{4}$$

$$\dot{I}_{L1} = \frac{1}{L_{L1}} V_{C_{L1}} u_3 - \frac{1}{L_{L1}} V_{L1} - \frac{R_{L1}+R_{03}}{L_{L1}} I_{L1} \tag{5}$$

$$\dot{V}_{C_{L1}} = \frac{1}{C_{L1}R'_{L1}}(V_{dc}-V_{C_{L1}}) - \frac{1}{C_{L1}} u_3 R_{03} I_{L1} \tag{6}$$

$$\dot{I}_{L2} = \frac{1}{L_{L2}} V_{C_{L2}} u_4 - \frac{1}{L_{L2}} V_{L2} - \frac{R_{L2}+R_{04}}{L_{L2}} I_{L2} \tag{7}$$

$$\dot{V}_{C_{L2}} = \frac{1}{C_{L2}R'_{L2}}(V_{dc}-V_{C_{L2}}) - \frac{1}{C_{L2}} u_4 R_{04} I_{L2} \tag{8}$$

$$\dot{V}_{dc} = \frac{1}{C_{dc}R'_{Bat}}(V_{C_{Bat}}-V_{dc}) + \frac{1}{C_{dc}R'_{PV}}(V_{C_{PV}}-V_{dc}) + \\ + \frac{1}{C_{dc}R'_{L1}}(V_{C_{L1}}-V_{dc}) + \frac{1}{C_{dc}R'_{L2}}(V_{C_{L2}}-V_{dc}) \tag{9}$$

where V_{Bat}, V_{PV}, V_{L1} and V_{L2} are the voltages on the battery, PV panel, load 1 and load 2, respectively. $V_{C_{Bat}}$, $V_{C_{PV}}$, $V_{C_{L1}}$ and $V_{C_{L2}}$ are the converter output voltages of each subsystem, while I_{Bat}, I_{PV}, I_{L1} and I_{L2} are the inductor currents of each subsystem. V_{dc} is the voltage on the DC bus, whereas u_1, u_2, u_3 and u_4 are the duty cycle of the converters. The converter inductance and capacitors of each system are denoted with L_{Bat}, $L_{C_{PV}}$, L_{L1} and $L_{C_{L2}}$ and C_{Bat}, $C_{C_{PV}}$, C_{L1} and $C_{C_{L2}}$, respectively. R'_{Bat}, R'_{PV}, R'_{L1} and R'_{L1} are the resistances representing the cable losses, while R_{01}, R_{02}, R_{03} and R_{04} represent the semiconductor losses.

III. control Strategy

The control aim of each converter is different. While the battery subsystem aims to control the DC-Bus voltage V_{dc} to the desired reference voltage $V^*_{dc} = 650V$, the PV is using a *Perturb and Observe MPPT* algorithm to achieve the maximum absorbed PV power. The load controllers are both controlling the load voltages V_{L1} and V_{L2} to their desired values $V^*_{L1} = 230V$ and $V^*_{L2} = 400V$. Assuming that the line resistance is $R_{Bat} \approx 0\Omega$, the DC bus voltage control assumes $V_{dc} = V_{C_{Bat}}$ and the control of the DC bus is equivalent to the control of $V_{C_{Bat}}$. The MPPT Algorithm used in both subsequent cases in Sec. III-A (PI-based control) and Sec. III-B (nonlinear control) is identical and a change of irradiance, temperature, and other effects are neglected for the sake of clarity.

A. PI-Control

In order to make a fair comparison of the control strategies, the PI controller is designed with a cascaded structure. The simplified block diagram of the PI controller to control voltage $V_{C_{Bat}}$ is depicted in Fig. 2. Note that the system dynamics are linearized around the equilibrium point $V^e_{dc} = 650V$, $V^e_{L1} = 230V$ and $V^e_{L2} = 400V$. The controlled voltages (V_{dc}, V_{L_1} and V_{L_2}) present a control structure with an outer control loop, that provides the reference for the inner control loop. Following the singular perturbation arguments (see [20]), the outer loop is designed to be slower than the inner one, where the difference between the dynamics, in the sense of time constants, in this case, is at least a decade, according to classical PI cascade controllers. The calculated control input for DC bus voltage control is presented in (10), where the current reference is provided by the voltage control loop in (11).

$$u_1 = -K_{p_2}(I_{Bat} - I^*_{Bat}) - K_{i_2}\int (I_{Bat} - I^*_{Bat})dt \tag{10}$$

$$I^*_{Bat} = -K_{p_1}(V_{C_{Bat}} - V^*_{C_{Bat}}) - K_{i_1}\int (V_{C_{Bat}} - V^*_{C_{Bat}})dt \tag{11}$$

Based on the block diagram in Fig. 2, considering the PI controller and the linearization of the plant, the closed-loop transfer function for DC bus voltage is obtained:

$$\frac{V_{dc}(s)}{V^*_{dc}(s)} = \frac{K_{p_1}s + K_{i_1}}{C_{dc}s^2 + K_{p_1}s + K_{i_1}} \tag{12}$$

Generally, the canonical form of the transfer function is expressed as:

$$F(s) = \frac{2\xi s + \omega_n^2}{s^2 + 2\xi\omega_n s + \omega_n^2} \tag{13}$$

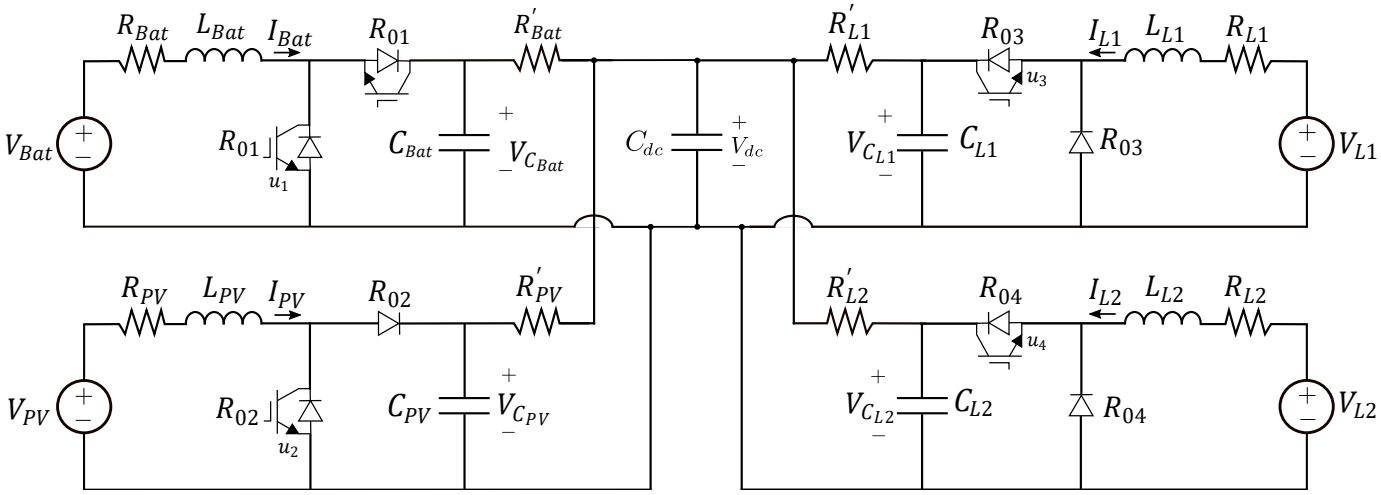

Fig. 1. DC MicroGrid circuit diagram consisting of a battery, PV, and two load busses.

where the damping coefficient $\xi = K_{p_1}/2\omega_n C_{dc}$ and the natural frequency $\omega_n = \sqrt{K_{i_1}/C_{dc}}$ can be adjusted to obtain the desired dynamical behavior with proper filtering. The gains of the PI controller can be calculated according to the chosen poles (p_1 and p_2) of the system, such that the voltage has desired dynamics. Therefore, the gains of the controller are given as:

$$s^2 + \frac{K_{p_1}}{C_{dc}}s + \frac{K_{i_1}}{C_{dc}} = (s+p_1)(s+p_2) = s^2 + (p_1+p_2)s + p_1p_2, \tag{14}$$

and can be calculated with:

$$K_{p_1} = C_{dc}(p_1+p_2) \quad ; \quad K_{i_1} = C_{dc}(p_1p_2). \tag{15}$$

The transfer function of the current control loop is provided as:

$$\frac{I_{Bat}(s)}{I^*_{Bat}(s)} = \frac{K_{p_2}s + K_{i_2}}{L_3s^2 + (R_{01}+K_{p_1})s + K_{i_1}} \tag{16}$$

considering the desired poles (p_3 and p_4) for the current dynamics, the gains of the controllers are calculated as:

$$K_{p_2} = L_{Bat}(p_3+p_4) - R_{01} \quad ; \quad K_{i_2} = L_{Bat}(p_3p_4). \tag{17}$$

B. Nonlinear Control

In this case, the control law of each device can be developed independently by feedback linearization technique, since each system has a different control target [21]. For the battery subsystem based on equation (1) the feedback linearization yields:

$$u_1 = \frac{1}{V_{C_{Bat}}}\left[L_{Bat}\phi_{Bat} - V_{Bat} + (R_{Bat}+R_{01})I_{Bat}\right] \tag{18}$$

with:

$$\phi_{Bat} = -K_{Bat}(I_{Bat} - I^*_{Bat}) - K^{\alpha}_{Bat}\alpha_{Bat}$$
$$\dot{\alpha}_{Bat} = I_{Bat} - I^*_{Bat}$$

where α_{Bat} is the integral term for zero error in steady state. The control of the output voltage on the battery subsystem is given by dynamic feedback linearization technique [21]. The boundary layer model of V_{C_1} dynamics is obtained considering I_{L_1} already in its equilibrium point $I^*_{L_1}$:

$$\dot{V}^*_{C_{Bat}} = \frac{V_{dc} - V^*_{C_{Bat}}}{C_{Bat}R'_{Bat}} - \frac{V_{Bat}I^*_{Bat}}{C_{Bat}V^*_{C_{Bat}}} + \frac{R'_{Bat}I^{*2}_{Bat}}{C_{Bat}V^*_{C_{Bat}}} \tag{19}$$

in steady-state. The second-order derivative leads to:

$$\ddot{V}^*_{C_{Bat}} = -(\kappa_1 + \frac{I_w}{R'_{Bat}C^2_{dc}}) + \kappa_2\dot{I}^*_{Bat} - \kappa_3 \tag{20}$$

with:

$$\kappa_1 = \frac{\dot{V}^*_{C_{Bat}}}{R'_{Bat}C_{Bat}} + \frac{V^*_{C_{Bat}} - V_{dc}}{{R'_{Bat}}^2 C_{Bat}C_{dc}}$$
$$\kappa_2 = \frac{V_{Bat} - 2(R_{Bat}+R_{01})I^*_{Bat}}{C_{Bat}V^*_{CBat}}$$
$$\kappa_3 = \frac{V_{Bat} + (R_{Bat}+R_{01})I^*_{Bat}}{C_{Bat}{V^*_{C_{Bat}}}^2}I^*_{Bat}\dot{V}^*_{CBat}$$

The term $\frac{I_w}{R'_{Bat}C^2_{dc}}$ is considered as a disturbance (from the grid) to be rejected. Considering $\dot{I}^*_{Bat}$ as the control input, the derivative of (19) is computed, obtaining the control input according to the feedback linearization procedure.

$$\dot{I}^*_{Bat} = \frac{\kappa_1 + \kappa_3}{\kappa_2} - v_1 \tag{21}$$

with:

$$v_1 = -K_{Bat}(V_{C_{Bat}} - V^*_{C_{Bat}}) - K^{\alpha}_{Bat}\alpha_1 \tag{22}$$

where α_1 is an integral term. The current reference is easily computed by integrating the control input $I^*_{Bat} = \int \dot{I}^*_{Bat}dt$. The voltage reference $V^*_{C_{Bat}}$ is calculated, such that V_{dc} is controlled to the desired reference V^*_{dc}, as introduced in the following:

$$V^*_{C_{Bat}} = R'_{Bat}\Big[v_{10} + \frac{V_{dc}}{R'_{Bat}} - \frac{1}{R'_{PV}}(V_{C_{PV}} - V_{dc}) +$$

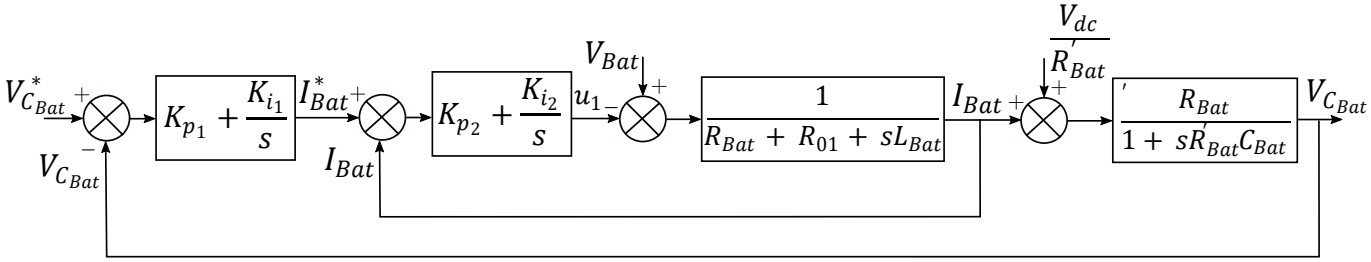

Fig. 2. Simplified block diagram of the PI controller for the DC bus.

$$-\frac{1}{R'_{L1}}(V_{C_{L1}} - V_{dc}) - \frac{1}{R'_{L2}}(V_{C_{L2}} - V_{dc})\Big] \quad (23)$$

with:

$$v_{10} = -K_{Bat_i}(V_{dc} - V^*_{dc}) - K^{\alpha}_{Bat_i}\alpha_{10} \quad (24)$$

where α_{10} is the integral term. System (1)-(2) is asymptotically stable at the desired equilibrium point under the control law (18) and of a reference trajectory for the current subsystem(21) in (19), which leads to full state transformation, achieving a linear second order system [7]. For the load subsystems, similar approaches are derived:

$$u_3 = \frac{1}{V_{C_{L1}}}\left[L_{L1}\phi_{L1} + V_{L1} - (R_{L1} + R_{03})I_{L1}\right] \quad (25)$$

$$u_4 = \frac{1}{V_{C_{L2}}}\left[L_{L2}\phi_{L2} + V_{L2} - (R_{L2} + R_{04})I_{L2}\right] \quad (26)$$

considering:

$$\phi_{L1} = -K_{L1}(I_{L1} - I^*_{L1}) - K^{\alpha}_{L1}\alpha_{L1} \quad (27)$$

$$\phi_{L2} = -K_{L2}(I_{L2} - I^*_{L2}) - K^{\alpha}_{L2}\alpha_{L2} \quad (28)$$

with ϕ_{L1} and ϕ_{L2} are the additional control designed such that a linear stable subspace is generated.

The integral terms α_{L1} and α_{L2} ensure zero error in steady state and can be written as: $\dot{\alpha}_{L1} = I_{L1} - I^e_{L1}$ and $\dot{\alpha}_{L2} = I_{L2} - I^e_{L2}$. The gains K_{L1},K^{α}_{L1}, K_{L2} and K^{α}_{L2} are positive constants and can be calculated by pole placement [7].

The voltage control loop provides the references for the inner current control loop. The time scale separation between the voltage and the current loop is given by placing the poles of voltages being much slower than the current subsystem. Therefore the singular perturbation condition [20] is created allowing the design of the controllers [6], [7]. The current references of the load 1 and 2 subsystems are provided as follows, such that the voltage are duly controlled:

$$I^*_{L_j} = -K_{Li,j}(V_{L_j} - V^*_{Lj}) - K^{\alpha}_{Li,j}\alpha_j \quad (29)$$

where $j = [1, 2]$, with α_j being integral terms.

IV. Experimental PHIL-Setup

The proposed nonlinear distributed control is verified by real-time PHIL tests shown in Fig. 3. The HIL system includes physical circuits realized by Silicon Carbide (SiC) MOSFETs (Type: NTHL020N120SC1). The switching frequency is chosen to be $20kHz$, which seems to be a good compromise between dynamics and efficiency[1]. The control algorithms

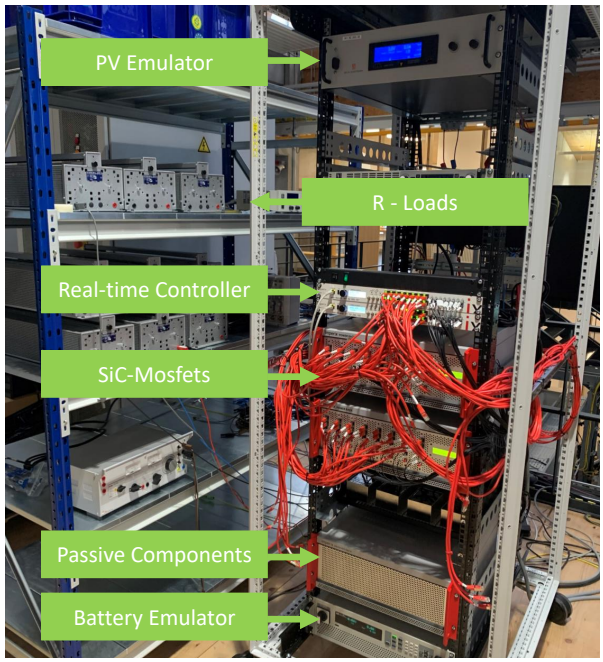

Fig. 3. Real-time PHIL setup consisting of PV Emulator, Loads, Real-time controller, SiC-Mosfets, passive Components and Battery Emulator.

are implemented in a real-time RAPID PROTOTYPING controller. The components parameters are listed in Table I.

TABLE I
MicroGrid parameters

Battery	PV	Load 1	Load 2	Value
R_{Bat}	R_{PV}	R_{L1}	R_{L2}	0.1 Ω
C_{Bat}	C_{PV}	C_{L1}	C_{L2}	$500\mu F$
R'_{Bat}	R'_{PV}	R'_{L1}	R'_{L2}	0.1 Ω
L_{Bat}	L_{PV}	L_{L1}	L_{L2}	2.5 mH
R_{01}	R_{02}	R_{03}	R_{04}	10 $m\Omega$

The PV array consists of polycrystalline IBC Solar PolySol with $3kWp$ of power in the nominal conditions, an open circuit voltage of $V_{OC} = 363.5V$, and a short circuit current of $I_{SC} = 5A$.

[1]High frequency = smaller size, faster transient response and smaller voltage over and undershoots, but increasing losses and heat and also more EMV problems.

V. Experimental Results

In this section, we present experimental results using the proposed nonlinear control method and the well-tuned PI controller, both introduced in Sec. III, implemented on a real-time PHIL DC Microgrid. Choosing the poles of the outer loop to $p_{1,2} = -100$ and the poles of the inner loop to $p_{3,4} = -500$ the calculation based on equation (15) and (17) leads to $K_{p1} = 0.4$, $K_{i1} = 20$, $K_{p2} = 2.5$ and $K_{i2} = 625$ for the battery subsystem. For the load, an equivalent calculation leads to $K_{p1} = 0.1$, $K_{i1} = 5$, $K_{p2} = 0.001$ and $K_{i2} = 0.1$. The calculations based on the nonlinear approach leads to $K_{Bat} = 10000$, $K^{\alpha}_{bat} = 200$, $K_{bat,i} = 25000$ and $K^{\alpha}_{bat,i} = 1000$ for the battery subsystem and to $K_{L1} = K_{L2} = 200$, $K^{\alpha}_{L1} = K^{\alpha}_{L2} = 10000$, $K_{Li,1} = K_{Li,2} = 1000$ and $K^{\alpha}_{Loadi.1} = K^{\alpha}_{Loadi.2} = 250000$. Note that the values of these gains are not equivalent, such as large or small values are not comparable.

At time $t = 50ms$, a load jump occurs which results in a doubling of the current and power demand. The DC voltage, load voltage, load current, and load duty cycle are depicted in Fig. 4 for the PI controller, and in Fig. 4 for the nonlinear controller. The comparison shows far better performance of the nonlinear control over the PI control. While the load step leads to a recognizable drop on the DC voltage V_{dc} as seen in the first plot of Fig. 4, the same load step has nearly no effect on the DC voltage V_{dc} of the nonlinear controlled DC grid as seen in Fig. 4. Furthermore, in Fig. 4 the load voltage V_{L1} needs around $1s$ to reach its steady state after the load step in the PI based grid, whereas the nonlinear control, on the other hand, is able to control the desired voltage into the steady state within around $0.1s$ as depicted in Fig. 4.

In Fig. 5 the response of PI controller after a change of the parameter K_{p2} from 0.001 to 0.0011 is shown. The response of a change of the nonlinear control parameter K^{α}_{L} from 200 to 100 is depicted in Fig. 6. While the nonlinear control keeps its stability properties, as can be seen in Fig. 6, even for a change in parameters, the PI-based control, on the other hand, already tends to get unstable at small deviations of the gains, as can be seen for instance in the load voltage, current and duty cycle in Fig. 5. From the results, it is obvious that the nonlinear controller is more robust to variations in the parameters. This has been experimentally established with many more experiments not shown in the present publication in view of limited space.

VI. Conclusion

The present paper introduces the development and experimental results of the control of a multi-terminal DC MicroGrid integrating RES, storage technology and electric vehicles in an urban environment. In this work, we present a DC MicroGrid architecture with a reduced amount of capacitors with respect to previous approaches. Further, we design a novel nonlinear control algorithm that is able to asymptotically stabilize all states to their references, even in the case of significant variation in equilibrium points and external variables, which are the main characteristics of renewables and EV's

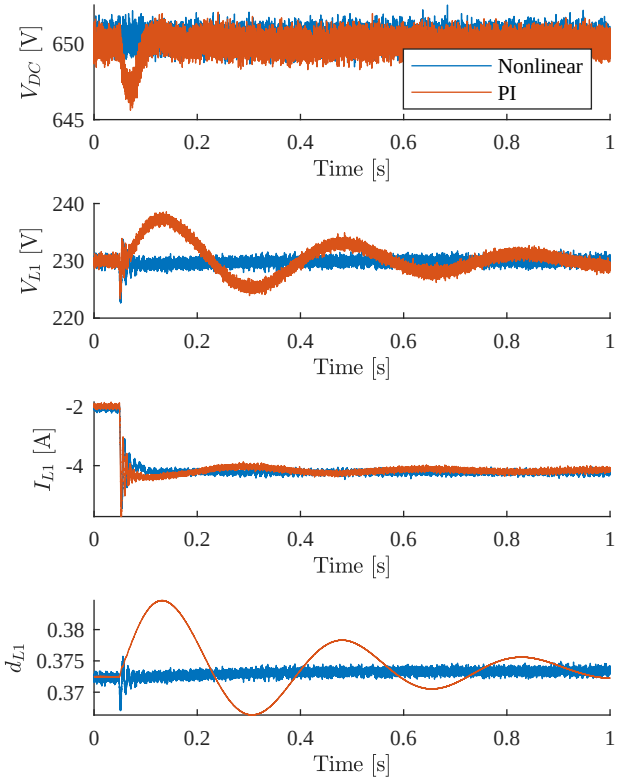

Fig. 4. Nonlinear (blue) and PI (red) controlled DC MicroGrid voltage, load's voltage, current and controller duty cycle during a load step at $t = 50ms$.

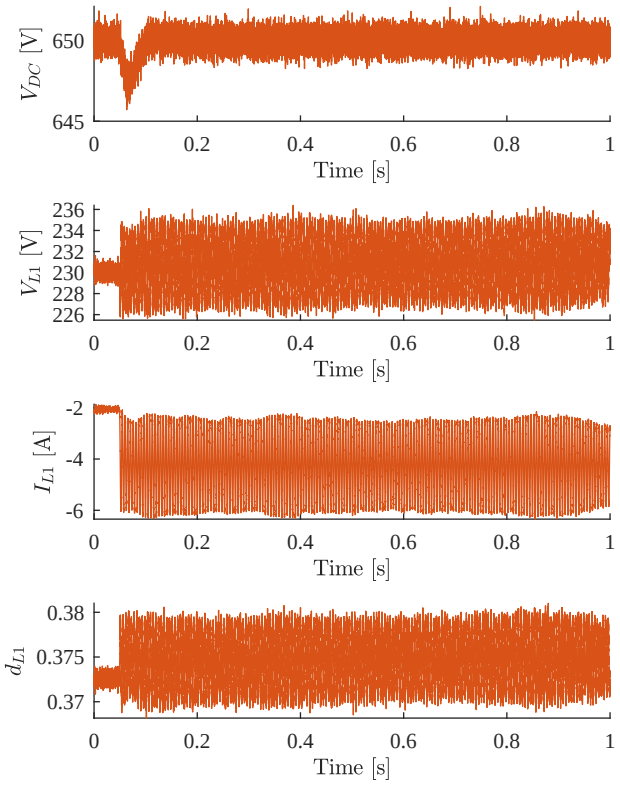

Fig. 5. PI controlled DC MicroGrid voltage, load's voltage, current and controller duty cycle during a load step at $t = 50ms$ after varying the Parameter K_{p2} from 0.001 to $= 0.0011$.

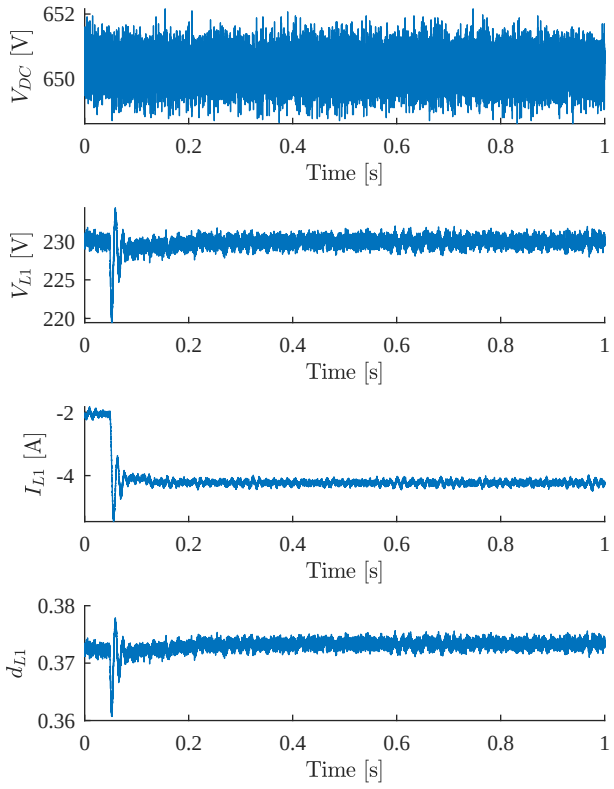

Fig. 6. Nonlinear controlled DC MicroGrid voltage, load's voltage, current and controller duty cycle during a load step at $t = 50ms$ after varying the Parameter K_L^{α} from 200 to 100 .

intermittence. The proposed controllers are then tested in a PHIL experimental setup, showing their good performance and robustness. The results are conclusive and illustrate the good performance of the nonlinear controllers. It is important to remark that, compared to the cascaded PI controllers, the proposed nonlinear controllers are much easier to be tuned in the experimental setup. In this light, using the nonlinear controllers it is possible to present several points of operation, and to better deal with perturbations and non-linearities of the system. Future works will address even more complex DC Microgrids, as well as their use to provide ancillary services to an AC grid. Furthermore, a rigorous stability verification will be added in future works.

ACKNOWLEDGMENT

The authors would like to thank Simon Waczowicz and Friedrich Wiegel and Alexander Höllhuber from the Energy Lab 2.0 and the Institute for Automation and Applied Informatics (IAI) at KIT for their support and many discussions.

REFERENCES

[1] G. R. Broday, L. A. C. Lopes, and G. Damm, "Exact feedback linearization of a multi-variable controller for a bi-directional dc-dc converter as interface of an energy storage system," *Energies*, vol. 15, no. 21, 2022.

[2] S. M. Ashabani and Y. A. r. I. Mohamed, "New family of microgrid control and management strategies in smart distribution grids; analysis, comparison and testing," *IEEE Transactions on Power Systems*, vol. 29, pp. 2257–2269, Sept 2014.

[3] V. A. Boicea, "Energy storage technologies: The past and the present," *Proceedings of the IEEE*, vol. 102, pp. 1777–1794, Nov 2014.

[4] H. Bevrani, B. François, and T. Ise, *Microgrid dynamics and control*. John Wiley & Sons, 2017.

[5] S. K. Sahoo, A. K. Sinha, and N. Kishore, "Control techniques in ac, dc, and hybrid ac-dc microgrid: a review," *IEEE Journal of Emerging and Selected Topics in Power Electronics*, vol. 6, no. 2, pp. 738–759, 2017.

[6] F. Perez and G. Damm, "Dc microgrids," in *Microgrids design and implementation*, pp. 447–475, Springer, 2019.

[7] F. Perez, A. Iovine, G. Damm, L. Galai-Dol, and P. F. Ribeiro, "Stability analysis of a dc microgrid for a smart railway station integrating renewable sources," *IEEE Transactions on Control Systems Technology*, 2019.

[8] M. Tucci, S. Riverso, J. C. Vasquez, J. M. Guerrero, and G. Ferrari-Trecate, "A decentralized scalable approach to voltage control of dc islanded microgrids," *IEEE Transactions on Control Systems Technology*, vol. 24, pp. 1965–1979, Nov 2016.

[9] T. Dragičević, X. Lu, J. C. Vasquez, and J. M. Guerrero, "Dc microgrids—part i: A review of control strategies and stabilization techniques," *IEEE Transactions on power electronics*, vol. 31, no. 7, pp. 4876–4891, 2015.

[10] L. Meng, Q. Shafiee, G. F. Trecate, H. Karimi, D. Fulwani, X. Lu, and J. M. Guerrero, "Review on Control of DC Microgrids and Multiple Microgrid Clusters," *IEEE Journal of Emerging and Selected Topics in Power Electronics*, vol. 5, pp. 928–948, Sept 2017.

[11] F. Perez, G. Damm, C. M. Verrelli, and P. F. Ribeiro, "Adaptive virtual inertia control for stable microgrid operation including ancillary services support," *IEEE Transactions on Control Systems Technology*, pp. 1–13, 2023.

[12] A. Emadi, A. Khaligh, C. Rivetta, and G. Williamson, "Constant power loads and negative impedance instability in automotive systems: definition, modeling, stability, and control of power electronic converters and motor drives," *IEEE Transactions on Vehicular Technology*, vol. 55, no. 4, pp. 1112–1125, 2006.

[13] S. Sen and V. Kumar, "Microgrid control: A comprehensive survey," *Annual Reviews in control*, vol. 45, pp. 118–151, 2018.

[14] D. I. Makrygiorgou and A. T. Alexandridis, "Stability analysis of dc distribution systems with droop-based charge sharing on energy storage devices," *Energies*, vol. 10, no. 4, p. 433, 2017.

[15] A. Bidram and A. Davoudi, "Hierarchical structure of microgrids control system," *IEEE Transactions on Smart Grid*, vol. 3, no. 4, pp. 1963–1976, 2012.

[16] N. Yang, B. Nahid-Mobarakeh, F. Gao, D. Paire, A. Miraoui, and W. Liu, "Modeling and stability analysis of multi-time scale dc microgrid," *Electric Power Systems Research*, vol. 140, pp. 906–916, 2016.

[17] M. Jiménez Carrizosa, A. Iovine, G. Damm, and P. Alou, "Droop-inspired nonlinear control of a dc microgrid for integration of electrical mobility providing ancillary services to the ac main grid," *IEEE Transactions on Smart Grid*, vol. 13, no. 5, pp. 4113–4122, 2022.

[18] F. Perez, G. Damm, and P. Ribeiro, *DC Microgrids for Ancillary Services Provision*, pp. 403–437. Cham: Springer International Publishing, 2022.

[19] F. Wiegel, J. Wachter, M. Kyesswa, R. Mikut, S. Waczowicz, and V. Hagenmeyer, "Smart energy system control laboratory – a fully-automated and user-oriented research infrastructure for controlling and operating smart energy systems," *at - Automatisierungstechnik*, vol. 70, pp. 1116 – 1133, 2022.

[20] P. Kokotović, H. K. Khalil, and J. O'Reilly, *Singular Perturbation Methods in Control: Analysis and Design*. Society for Industrial and Applied Mathematics, 1999.

[21] H. K. Khalil, *Nonlinear control*, vol. 406. Pearson New York, 2015.